Cell Stem Cell

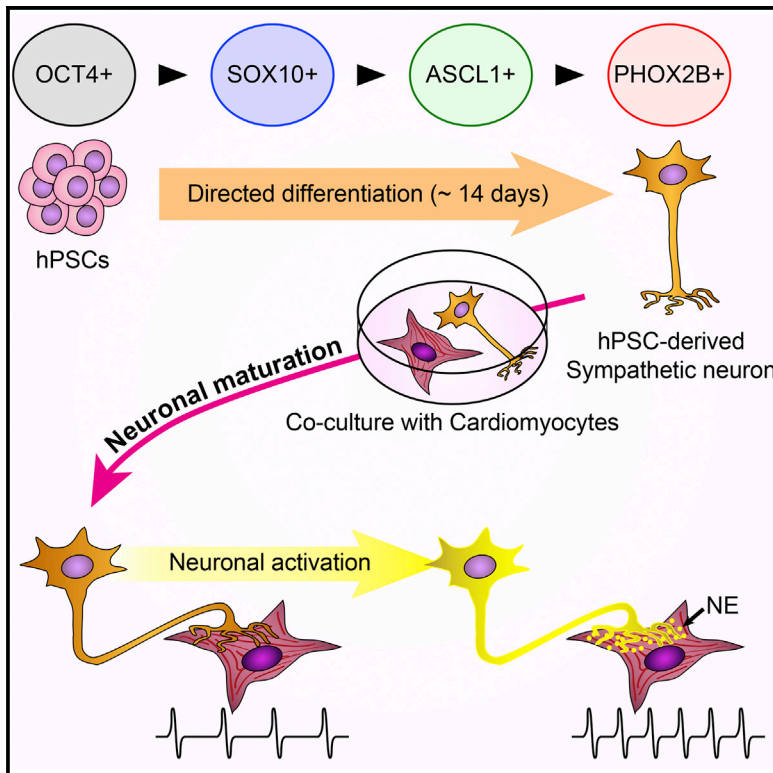# Functional Coupling with Cardiac Muscle Promotes Maturation of hPSC-Derived Sympathetic Neurons

Graphical Abstract

Highlights

- Norepinephrine-secreting sympathetic neurons differentiated from human PSCs

- Sympathetic neurons functionally couple with cardiac tissue in vitro

- Pharmacological and optogenetic control of neuronal activity tunes myocyte beating

- Co-culture with cardiac tissues enhances neuronal maturation

Authors

Yohan Oh, Gun-Sik Cho, Zhe Li, ..., Xinzhong Dong, Chulan Kwon, Gabsang Lee

Correspondence

ckwon13@jhmi.edu (C.K.),
glee48@jhmi.edu (G.L.)

In Brief

Oh et al. differentiate human pluripotent stem cells into functional sympathetic neurons that can functionally and physically couple with ventricular cardiomyocytes. This coupling controls cardiomyocyte beating and promotes neuronal maturation, providing a platform for studying neuronal regulation of cardiac behavior and modeling complex intercellular physiology.

Accession Numbers

GSE80689

CrossMark

CellPress

Functional Coupling with Cardiac Muscle Promotes Maturation of hPSC-Derived Sympathetic Neurons

Yohan Oh,[1,2,3] Gun-Sik Cho,[1,4] Zhe Li,[5] Ingie Hong,[5] Renjun Zhu,[6] Min-Jeong Kim,[1,2,9] Yong Jun Kim,[1,2,10] Emmanouil Tampakakis,[4] Leslie Tung,[6] Richard Huganir,[5] Xinzhong Dong,[5,7,8] Chulan Kwon,[1,4,*] and Gabsang Lee[1,2,3,5,*]

[1]Institute for Cell Engineering
[2]Department of Neurology
Johns Hopkins University School of Medicine, Baltimore, MD 21205, USA
[3]Adrienne Helis Malvin Medical Research Foundation, New Orleans, LA 70130, USA
[4]Division of Cardiology
[5]The Solomon H. Snyder Department of Neuroscience
[6]Department of Biomedical Engineering
[7]Center for Sensory Biology
Johns Hopkins University School of Medicine, Baltimore, MD 21205, USA
[8]The Howard Hughes Medical Institute, Baltimore, MD 21205, USA
[9]Present address: Stem Cell & Regenerative Medicine Institute, Research Institute for Future Medicine, Samsung Medical Center, Seoul 06351, Korea
[10]Present address: Department of Pathology, College of Medicine, Kyung Hee University, Seoul 130-701, Korea
*Correspondence: ckwon13@jhmi.edu (C.K.), glee48@jhmi.edu (G.L.)
http://dx.doi.org/10.1016/j.stem.2016.05.002

SUMMARY

Neurons derived from human pluripotent stem cells (hPSCs) are powerful tools for studying human neural development and diseases. Robust functional coupling of hPSC-derived neurons with target tissues in vitro is essential for modeling intercellular physiology in a dish and to further translational studies, but it has proven difficult to achieve. Here, we derive sympathetic neurons from hPSCs and show that they can form physical and functional connections with cardiac muscle cells. Using multiple hPSC reporter lines, we recapitulated human autonomic neuron development in vitro and successfully isolated PHOX2B::eGFP+ neurons that exhibit sympathetic marker expression and electrophysiological properties and norepinephrine secretion. Upon pharmacologic and optogenetic manipulation, PHOX2B::eGFP+ neurons controlled beating rates of cardiomyocytes, and the physical interactions between these cells increased neuronal maturation. This study provides a foundation for human sympathetic neuron specification and for hPSC-based neuronal control of organs in a dish.

INTRODUCTION

Sympathetic neurons originate from neural crest cells and control the functions of vital organs as part of the autonomic nervous system (ANS) (Anderson et al., 1997; Bhatt et al., 2013). When the sympathoadrenal neural crest cells migrate along the ventromedial path, they are exposed to the morphogens sonic hedgehog proteins (SHH) and bone morphogenetic proteins (BMP) sequentially, which are secreted from the notochord and aorta region, respectively (Anderson et al., 1997; Bhatt et al., 2013). The migrated neural crest cells initially form a continuous sympathetic chain. This chain segregates into discrete ganglia and differentiates into sympathetic neurons that innervate various targets, including cardiac tissues, blood vessels, glands, and smooth muscle (Bhatt et al., 2013; Takahashi et al., 2013). Aberrant activity and dysfunction of the sympathetic neurons contribute to the pathophysiology of human hypertension and cardiac conditions (Kimura et al., 2012), diabetes mellitus (Vinik et al., 2003), Parkinson's disease (Chaudhuri, 2001), and familial dysautonomia (Axelrod et al., 2002; Rotthier et al., 2012).

Although animal models are widely used to study human autonomic neurons and related disorders, they have significant limitations due to the inter-individual genetic heterogeneity and distinct homeostatic mechanisms between rodents and humans. Neurons derived from human pluripotent stem cells (hPSCs), including embryonic stem or induced pluripotent stem cells (hESCs/hiPSCs), have emerged as a promising model for studying human neural development and disease (Brennand et al., 2011; Dimos et al., 2008; Laflamme et al., 2007; Li et al., 2005; Maroof et al., 2010) and could be used as cell sources for transplantation (Cunningham et al., 2014; Joseph and Morrison, 2005). While significant and rapid progress has been made on the generation and utilization of CNS cell types differentiated from hPSCs (Li et al., 2005; Perrier et al., 2004), very few studies have been reported on peripheral neural derivation (Lee et al., 2007; Schrenk-Siemens et al., 2015). Moreover, it remains unknown whether a defined population of peripheral neurons can be isolated from hPSCs. Although a recent report presented the generation of a functional neuromuscular junction using hPSCs-derived spinal motor neurons and skeletal muscle fibers (Steinbeck et al., 2016), it remains unknown whether hPSC-derived peripheral neurons can mimic neuromodulatory function with their target tissues.

Creating a reporter knockin system in hPSCs is a powerful approach for monitoring hPSC differentiation toward specific cell types and for isolating the resulting cells. The CRISPR/Cas9 system (Cong et al., 2013; Mali et al., 2013) offers targeted genome editing and can be used to efficiently generate hPSC lines harboring gene reporters. This can be applied for monitoring the development of a specific subtype of neurons, which would be beneficial for the studies of human sympathetic neuronal development and related human diseases.

Here, we recapitulated the sympathoadrenal differentiation process in vitro by developing multiple genetic reporters and demonstrated the successful differentiation and isolation of sympathetic progenitors and neurons from hPSCs. The sympathetic neuron identity was confirmed by gene expression analysis and physiological and functional activity. Furthermore, the resulting neurons showed physical and functional connectivity with heart muscle cells, leading to neuronal maturation.

RESULTS

WNT and SHH Signaling Enhance Both Expression Levels of ASCL1 and PHOX2B in hPSC-Derived Autonomic Specification

The basic helix-loop-helix (bHLH) transcription factor ASCL1 and homeodomain transcription factor PHOX2B are key transcription factors essential for sympathetic neuronal development (Hirsch et al., 1998; Pattyn et al., 2000). To test whether sympathetic neurons can be induced from hPSCs, we established two genetic reporter lines expressing GFP from the loci of *ASCL1* and *PHOX2B*, i.e., *ASCL1::eGFP* and *PHOX2B::eGFP* hESCs (Figures 1A–1F). The gene targeting strategy was to replace each stop codon of the *ASCL1* and *PHOX2B* genes with 2A-eGFP-PGK-Puro^R gene cassettes through homologous recombination enhanced by the CRISPR/Cas9 system (Cong et al., 2013; Mali et al., 2013) (Figures 1A and 1D). After selecting phenotypically and karyotypically normal lines (Figures 1B, 1E, S1A, and S1B), we searched for sympathetic neuronal differentiation. In animal models, specification of sympathetic neurons and chromaffin cells are specified from migrating neural crest stem cells by SHH and BMP signaling (Morikawa et al., 2009; Schneider et al., 1999). We initially induced neural crest cells using SMAD inhibition (termed "LSB" for inhibitors LDN193189 and SB431542) protocol (Chambers et al., 2009). Similar to the in vivo process, expression levels of ASCL1::eGFP and PHOX2B::eGFP were significantly enhanced with recombinant sonic hedgehog C25II (Shh) protein and SHH agonist (purmorphamine, PMP) and significantly decreased by treatment with an SHH antagonist (cyclopamine, CyP) (Figures 1G, S1C, and S1D). In addition, BMP4 treatment from day 10 significantly increased the expression of ASCL1 and PHOX2B (Figure 1H). Mica et al. (2013) showed that WNT activation using CHIR99021 combined with the LSB method augments the proportion of neural crest cells in the population. Similarly, we also found that transient WNT activation (started 1 day before the activation of SHH signaling) induces both ASCL1::eGFP and PHOX2B::eGFP expression (Figure 1I). To accelerate neural crest specification and peripheral neuron formation from neural crest cells, we adopted the combined three

small molecules protocol (CHIR99021, DAPT, and SU5402, called "3i" for "three inhibitors") (Chambers et al., 2012) and modified it with substitution of PD173074 for SU5402 (modified-3i or m3i). We observed significantly higher levels of ASCL1::eGFP and PHOX2B::eGFP expression with the m3i treatment than with the CHIR99021 single treatment (Figure 1I). The numbers of ASCL1::eGFP and PHOX2B::eGFP cells were also greatly increased with m3i treatment followed by BMP4 (46.43 ± 0.54% and 4.13 ± 0.18%, respectively) (Figure 1J). The eGFP expression of both reporter lines was detectable either by the fluorescence-activated cell sorting (FACS) analysis, immunocytochemistry, or live cell imaging and mostly co-localized with endogenous ASCL1 or PHOX2B proteins (Figures 1C, 1F, 1K, and S1E–S1G). Some PHOX2B-expressing cells began to show neurite outgrowth from day 10 after differentiation (Figures 1K, right, and S1G). Post-sorting quantitative (q)RT-PCR showed the enrichment of transcripts expressed in sympathetic neuron and/or chromaffin cells specification, indicating a proper lineage specification (Figure 1L). We further generated a *PHOX2B::eGFP* reporter hiPSC line and produced PHOX2B::eGFP+ cells from hiPSCs using the same neuronal specification protocol (Figure S1H). Together, these results showed that the activation of WNT followed by SHH signaling leads to the generation of both *ASCL1*- and *PHOX2B*-expressing sympathetic progenitors and neurons from hPSCs.

Global Gene Expression Changes during Sympathetic Neuronal Differentiation

The dynamics of global gene expression during sympathoadrenal differentiation remains largely unknown even in animal models. Using the four genetic reporter systems (*OCT4::eGFP* [Figure S1I], *SOX10::eGFP* [Figure S1J], *ASCL1::eGFP*, and *PHOX2B::eGFP* reporter hESC lines), we were able to purify discrete cell populations at four differentiation stages, recapitulating the sympathoadrenal differentiation process in vitro with purified and defined populations in four specific differentiation stages (Figure 2A). We performed transcriptome analysis of OCT4::eGFP+ cells (representing undifferentiated hESCs), SOX10::eGFP+ cells (multi-potent neural crest), ASCL1::eGFP+ cells (putative sympathoadrenal progenitors), and PHOX2B::eGFP+ cells (putative sympathetic neuronal precursors) shown by the hierarchically clustering heatmap (Figure 2B). Each of the four purified populations had unique gene expression patterns associated with their cellular identities (Figures 2C–2F and S2A–S2D). Other groups have reported that *ASCL1* and *PHOX2B* are genetically correlated with each other during murine ANS development (Hirsch et al., 1998; Huber et al., 2002; Pattyn et al., 2000). Consistently, our data also demonstrated that ASCL1::eGFP+ and PHOX2B::eGFP+ cells share similar patterns of gene expression (Figures 2B and 2E). However, gene ontology (GO) analysis and differential gene expression data indicated that ASCL1::eGFP+ cells are specified earlier than PHOX2B::eGFP+ cells during sympathetic neuronal development (Figures 2F–2H, S2C, S2D, and S2G). Additionally, we verified sets of transcriptomes that are associated with the specification of sympathoadrenal lineage cells (Figures 2E and S2A–S2C) and identified signature genes involved in the sympathetic neuronal specification (Figures 2F and S2D) and gene sets of two relevant diseases (dysautonomia and neuroblastoma) (Figures S2E and S2F). ASCL1::eGFP+ and
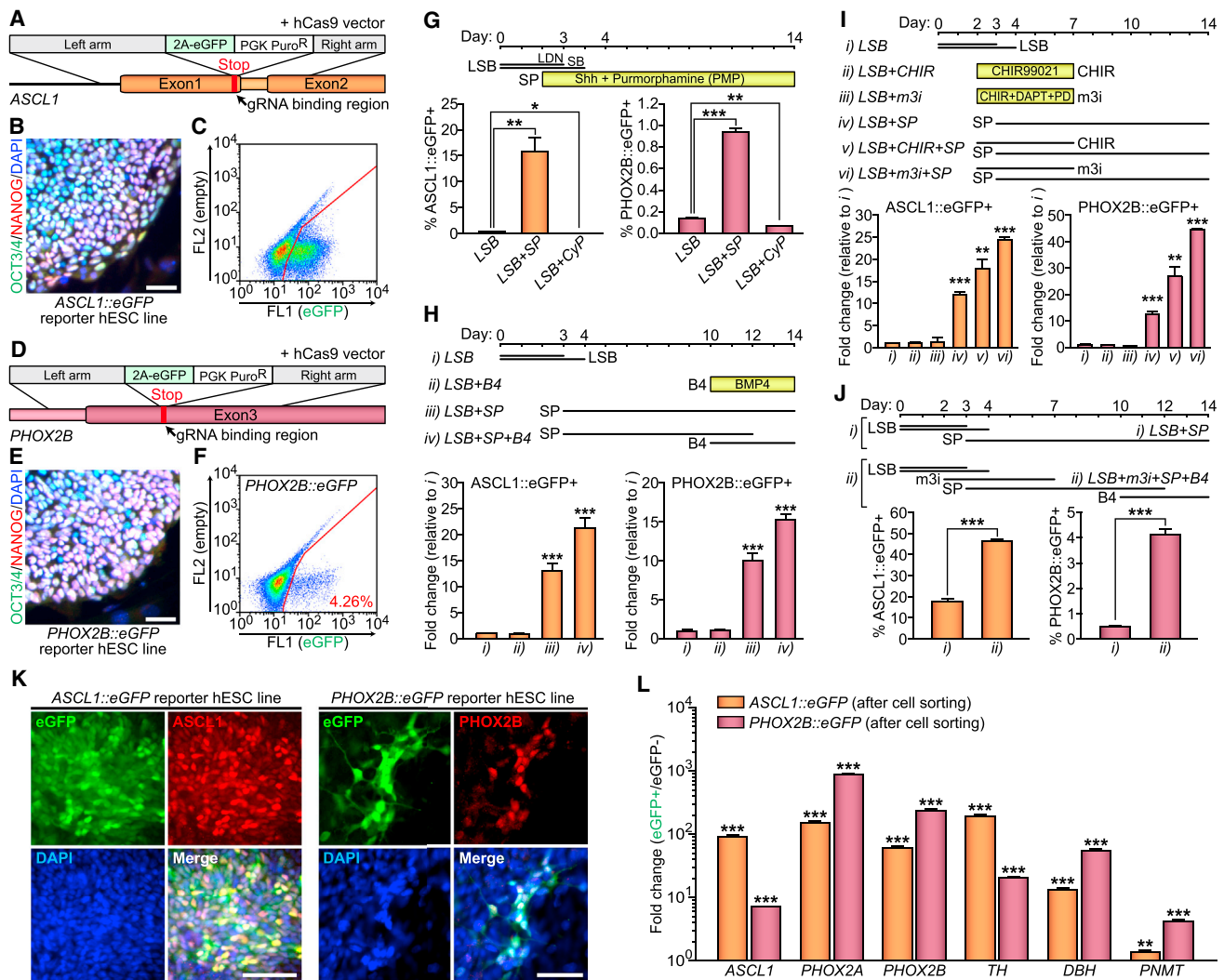
Figure 1. Activation of WNT followed by SHH Signaling Leads Both ASCL1 and PHOX2B Inductions in hPSC-Derived Autonomic Specification

(A and D) Schematics for *ASCL1* (A) and *PHOX2B* (D) gene targeting using homologous recombination enhanced by CRISPR/Cas9 system.

(B and E) Immunofluorescence analyses were performed using OCT3/4 (green) and NANOG (red) antibodies. The representative images of OCT3/4+/NANOG+ colonies from the undifferentiated *ASCL1::eGFP* (B) and *PHOX2B::eGFP* (E) reporter lines are shown.

(C and F) Representative FACS plots of differentiated reporter hESC lines for either *ASCL1* (C) or *PHOX2B* (F).

(G–J) Top, schematics for differentiation; bottom, after addition of the Shh protein and PMP or CyP to the LSB protocol (G), BMP4 (B4) to the LSB-SP protocol (H), CHIR99021 (CHIR) and m3i (CHIR, DAPT, and PD173074) to the LSB-SP protocol (I), or m3i and B4 to the LSB protocol (J), the percentages of ASCL1::eGFP- and PHOX2B::eGFP-expressing cells were measured by using FACS analysis (*p < 0.05; **p < 0.01; ***p < 0.001; unpaired Student's t test; and n = 3) (LSB, LDN193189, and SB431542) (SP and Shh plus PMP).

(K) Immunofluorescence analyses were performed at day 10 following LSB (day 0–3/4) - m3i (day 2–7) - SP (day 3–10) treatment, using GFP (green) and either ASCL1 (red) or PHOX2B (red) antibodies.

(L) qRT-PCR data showing enrichments of each transcript after cell sorting (**p < 0.01; ***p < 0.001; compared to eGFP- population; unpaired Student's t test; and n = 3).

All of the error bars represent mean + SEM. The scale bars represent 50 μm. See also Figure S1.

PHOX2B::eGFP+ cells expressed higher levels of PNMT and chromogranin A (CHGA) (Figures 1L and 2E), suggesting the presence of sympathoadrenal progenitors (Huber, 2015). Indeed, these cells could give rise not only to sympathetic neuronal cells, but also to "chromaffin-like" cells (Figure S2H). Together, these data show the feasibility of modeling human sympathetic development with hPSCs.

Characterization of PHOX2B::eGFP+ Neurons from hPSCs

With this established protocol, we successfully guided hPSCs to become putative sympathetic neurons (Figure 3). Sorted PHOX2B::eGFP+ cells were further differentiated into PHOX2B, peripherin (PRPH), TH, DBH, GATA3, ISL1, and nicotinic acetyl-choline receptors (nAChRs)-expressing putative sympathetic
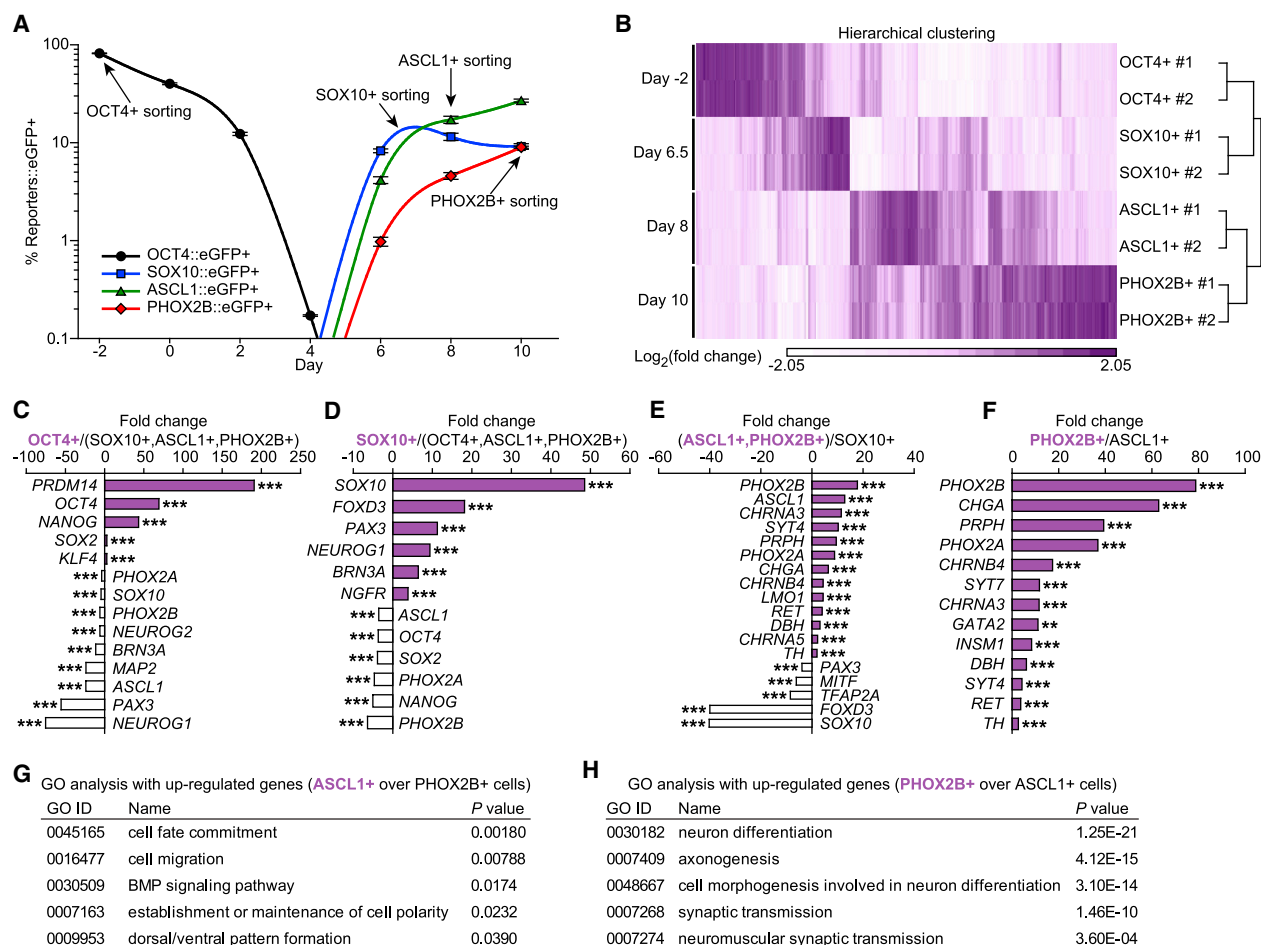
Figure 2. Genetic Reporter hPSC Lines for Four Different Genes Reveal Distinct Stages of Sympathetic Neuronal Differentiation

(A–H) Changes of each reporter gene expression after differentiation using different lines and protocols: for *OCT4::eGFP* and *SOX10::eGFP* lines: LSB (day 0–3/4) - CHIR (day 2–10); for *ASCL1::eGFP* line: LSB (day 0–3/4) - CHIR (day 2–7) - SP (day 3–10); and for *PHOX2B::eGFP* line: LSB (day 0–3/4) - m3i (day 2–7) - SP (day 3–10). The eGFP positive samples were collected by cell sorting at the specific time points as indicated (LSB, LDN193189, and SB431542; m3i, CHIR [CHIR99021], DAPT, and PD173074; and SP and Shh plus PMP).

(B) Clustered heatmap of global gene expression after microarray analyses (n = 2).

(C–F) List of the increased (purple) and decreased (white) genes comparing two groups, as assessed by microarray analysis (**p < 0.01; ***p < 0.001; ANOVA test using Partek Genomics Suite [Partek Inc.]; n = 3 for OCT4+, SOX10+, or ASCL1+ cells; and n = 2 for PHOX2B+ cells).

(G and H) GO analysis with upregulated gene list (G, ASCL1+ cells over PHOX2B+ cells and H, PHOX2B+ cells over ASCL1+ cells).

All of the error bars represent mean ± SEM. See also Figure S2.

neurons (Figures 3A–3C and S3A–S3D). These cells expressed sympathetic neuronal genes after differentiation (Figure 3D) and showed negligible percentages of HB9-expressing motor neurons (0.54 ± 0.42% of cells) and BRN3A-expressing sensory neurons (0.89 ± 0.28% of cells) (Figures S3E, S3F, and S3J). Based on this information, we were able to obtain sympathetic neurons without cell sorting. Differentiated parental hPSCs (genetically unmodified) could give rise to cells expressing ASCL1 and PHOX2B (Figure S3K) and subsequently yield TH/DBH/GATA3/PRPH-expressing and catecholamines-releasing neurons from hPSCs (Figures S3M–S3P) with a similar protocol as described (Figure S3L). In addition, FACS-purified ASCL1::eGFP+ cells were maintained over 150 days and differentiated into ASCL1/TH/DBH/GATA3/PRPH-expressing neurons (Figures S3Q–S3V). To test whether the neurons differentiated from sorted PHOX2B::eGFP+ cells were electrophysiologically functional, we subse-

quently performed a whole-cell patch-clamp analysis. As shown in Figure 3E, these neurons expressed a considerable amount of Na^+ channels and K^+ channels for conducting both inward and outward currents. These neurons were able to fire an action potential (AP) train when 50 mM KCl was added to the bath (Figure 3F), and the hESC-derived putative sympathetic neurons also responded to nicotine, which directly binds and activates nAChRs of post-ganglionic sympathetic neurons (Figures S3G and S3H). Upon current injecting, the neurons fired a single AP (Figure 3G, left; Type 1, "phasic") or a train of APs (Figure 3G, right; Type 2, "tonic") and exhibited a medium after hyperpolarization (AHP) (Figure 3H), the amplitude and duration of which were 12.1 ± 1.2 mV and 291.1 ± 55.8 ms, respectively (n = 3) and had the resting membrane potential (RMP) of −46.2 ± 5.4 mV (n = 12) in sorted PHOX2B::eGFP+ cells. We tested whether the depolarization of these neurons was dependent on Ca^{2+} and/or
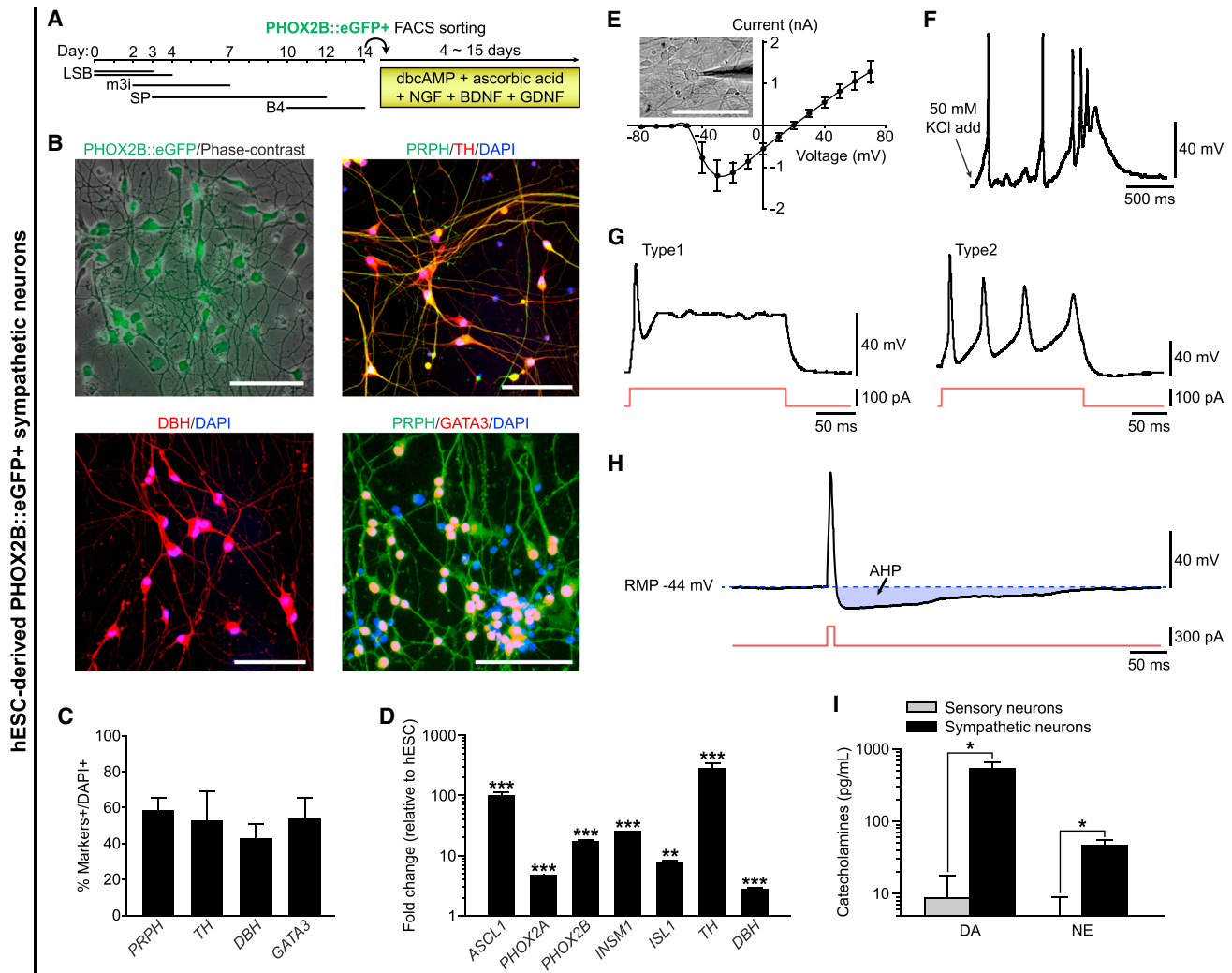
Figure 3. Characterization of FACS-Purified PHOX2B::eGFP+ Sympathetic Neurons from hPSCs

(A) Schematic for differentiation of PHOX2B::eGFP positive cells (LSB, LDN193189, and SB431542; m3i, CHIR99021, DAPT, and PD173074; and SP and Shh plus PMP, B4, and BMP4).

(B) FACS-purified PHOX2B::eGFP-expressing putative sympathetic neuronal precursors gave rise to PRPH (pseudo-green), TH (red), DBH (red), and GATA3 (red)-expressing sympathetic neurons.

(C) Quantification of PRPH, TH, DBH, and GATA3 positive cells (n = 3).

(D) qRT-PCR data showing significant increases of each transcript after sympathetic neuronal differentiation ($**p < 0.01$; $***p < 0.001$; compared to each transcript level of undifferentiated hESCs; unpaired Student's t test; and n = 3).

(E–H) Electrophysiological characterization of PHOX2B::eGFP-expressing sympathetic neurons, including I-V curve (n = 7) (E), representative APs upon either administration of 50 mM KCl (F) or injecting 100 pA current (G) or injecting 300 pA current (H).

(E) 10 of 10 neurons express a considerable amount of sodium channels and potassium channels to conduct both inward and outward current.

(F) 3 of 4 neurons responded to 50 mM KCl.

(G) 4 of 9 neurons fired a single of AP (Type 1), and 5 of 9 neurons fired a train of APs (Type 2), 8 of 9 neurons responded to currents of 100 pA or greater, and 1 (Type 1) of 9 neurons responded to currents of 300 pA or greater.

(H) An AP (top) evoked during a brief depolarizing current step (bottom), with an AHP, 3 of 4 neurons had medium AHP (lasts 221–428 ms) (RMP).

(I) Release of catecholamines after 50 mM KCl administration were analyzed by using a commercial ELISA kit ($*p < 0.05$; unpaired Student's t test; and n = 3) (DA and NE).

All of the error bars represent mean ± SEM or mean + SEM. The scale bars represent 100 μm. See also Figure S3.

Na$^+$ ions. As expected, the AP of these neurons was partially blocked with Cd^{2+} (non-specific Ca^{2+} channel blocker) alone and completely blocked with Cd^{2+} + TTX (voltage-dependent Na$^+$ channel blocker), showing the dependence on both Ca^{2+} and Na$^+$ ions (Figure S3I). These data suggest hPSC-derived sym-

pathetic neurons possess electrophysiological properties similar to rodent sympathetic neurons (Anderson et al., 2001; Jobling and Gibbins, 1999). Finally, we found that the PHOX2B::eGFP+ neurons released significantly higher levels of dopamine (DA) and norepinephrine (NE), of which levels were significantly higher
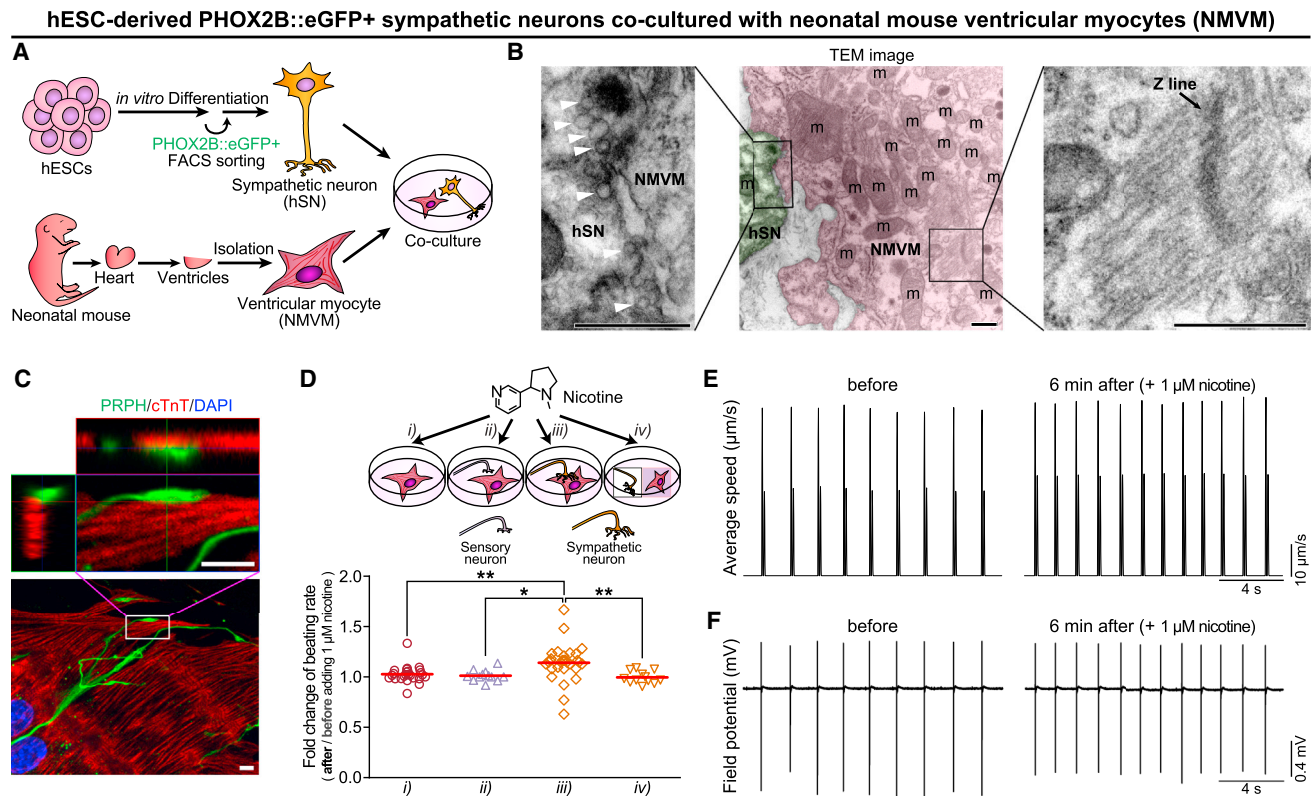
hESC-derived PHOX2B::eGFP+ sympathetic neurons co-cultured with neonatal mouse ventricular myocytes (NMVM)

Figure 4. hPSC-Derived Sympathetic Neurons Can Pharmacologically Control Spontaneous Beating of NMVM

(A) Schematic representation of the in vitro co-culture system, with FACS-purified human ESC-derived PHOX2B::eGFP+ sympathetic neurons (hSNs) and NMVM, used to test sympathetic-cardiac connections.

(B) Transmission electron microscopy (TEM) image of the junctional region between hSN and NMVM following co-culture. The green-colored region indicates the nerve terminal of a hSN, and the pink-colored region indicates the NMVM. The white arrowheads indicate putative synaptic vesicles.

(C) Immunofluorescence analysis was performed using PRPH (pseudo-green, hSNs) and cTnT (red, NMVM) antibodies. The maximum intensity projection of confocal microscopy z stacks are shown (bottom). The ortho-images of the boxed region in the bottom image are shown (top) (see Movie S1 for 3D reconstructed image).

(D) Top, schematic diagrams for the control of beating rate of NMVM; bottom, increased beating rates were observed upon the administration of 1 μM nicotine (see Experimental Procedures; *p < 0.05; **p < 0.01; unpaired Student's t test; and n = 25 for *i*, 12 for *ii*, 31 for *iii*, and 12 for *iv*). The red lines indicate each mean value.

(E and F) High speed video image acquisitions (E) and multi-electrode array (MEA) (F) recordings were synchronized (see Supplemental Information for more details). (E) Using motion vector analysis, increased beating rates were observed 6 min after administration of 1 μM nicotine. The first peaks of each beating indicate contractions, and the second peaks indicate relaxations. (F) Using MEA recordings, increased beating rates were detected 6 min after treatment of 1 μM nicotine.

The scale bars in (B) TEM images represent 0.5 μm and in (C) confocal images represent 5 μm. See also Figure S4 and Movies S1, S2, and S3.

than in hESC-derived PRPH/ISL1/BRN3A/RUNX1-expressing sensory neurons (Figures 3I and S3J). Taken together, these results demonstrate the feasibility of directing hPSCs into functional NE-secreting sympathetic neurons in vitro.

Pharmacological Neural Control of Cardiac Ventricular Myocytes

To examine neuronal functionality and to test sympathetic connections in vitro, we co-cultured FACS-purified PHOX2B::eGFP+ sympathetic neurons with neonatal mouse ventricular myocytes (NMVM), mESC-, or hiPSC-derived cardiomyocytes (Figures 4A and S4A–S4I). Through morphological, ultrastructural, and immunofluorescence analyses, we found that the neurons form direct physical contact with cardiomyocytes (Figures 4B, 4C, and S4A–S4I; Movie S1). In particular, as shown in transmission electron microscopy (Figure 4B), hPSC-derived PHOX2B::

eGFP+ neurons started to form synaptic connections with a few putative synaptic vesicles, although their synaptic structure appeared to be underdeveloped. To address whether these connections can be made with other cell types, we co-cultured the neurons and C2C12 skeletal myotubes as a negative control (Figures S4J and S4K). We only detected one SV2 positive myotube out of 412 myotubes, suggesting that the hPSC-derived sympathetic neurons may have target specificity. We found that nicotine treatment (1 μM, stimulating sympathetic neurons only) affected the beating rate of NMVM in the presence of the hESC-derived sympathetic neurons (Figures 4D, iii, 4E, and 4F). However, the effect was not observed in any of the four control groups: NMVM only (Figure 4D, i), sensory neurons with NMVM (Figure 4D, ii), co-cultured on separate coverslips (Figure 4D, iv), or NMVM cultured with the conditioned medium of activated sympathetic neurons (Figure S4N), indicating that the direct
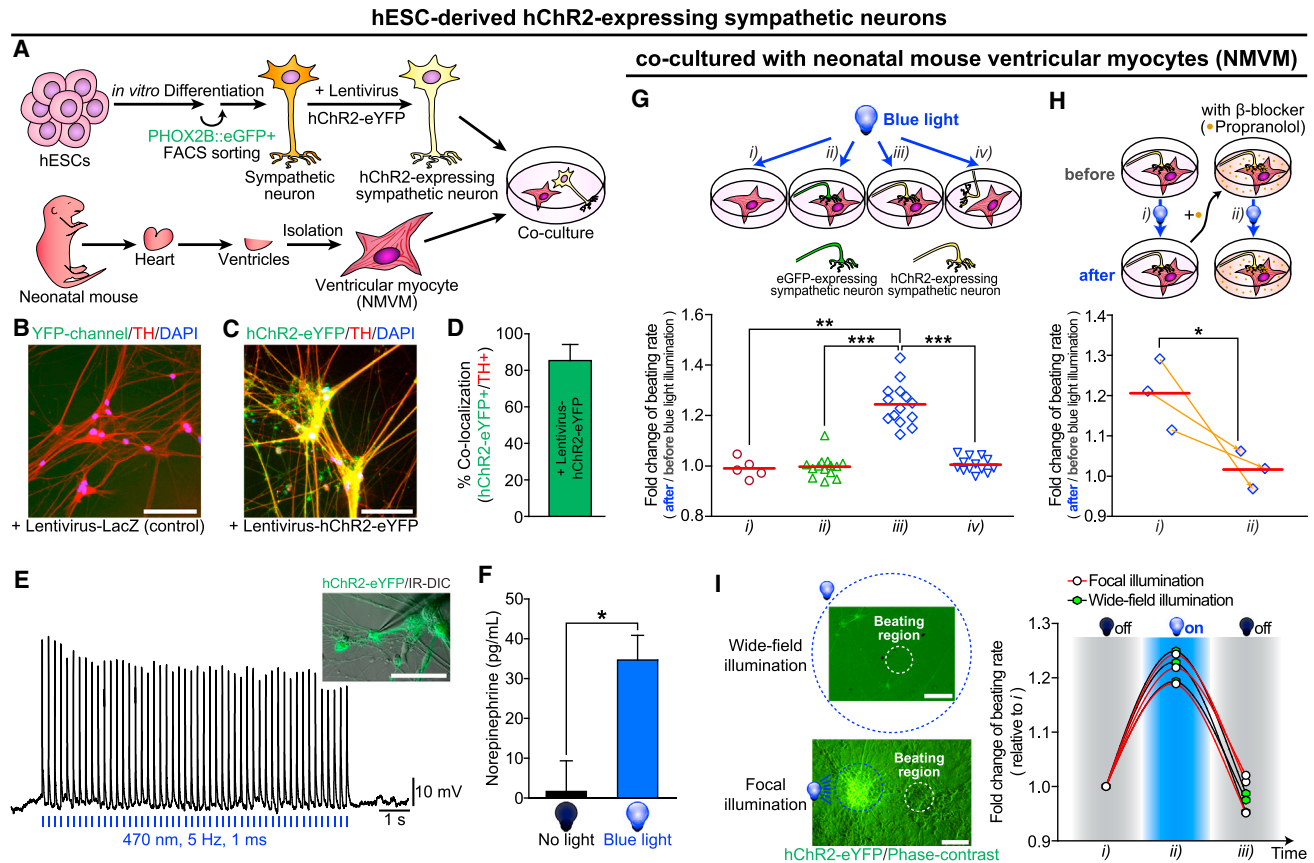
Figure 5. Optogenetic Control of hPSC-Derived Sympathetic Neurons Leads to Changes of Spontaneous Beating of NMVM

(A) Schematic representation of the in vitro co-culture system, with FACS-purified human ESC-derived hChR2-expressing PHOX2B::eGFP+ sympathetic neurons and NMVM, for testing sympathetic-cardiac connections. The hESC-derived sympathetic neurons were infected with hChR2 (C–I) or LacZ lentivirus (B).

(B and C) Immunofluorescence analyses were performed using TH (red) antibody.

(D) Quantification of the proportion of co-localized cells (n = 6).

(E) Cultured sympathetic neurons-expressing hChR2-eYFP were targeted in IR-DIC for whole-cell patch-clamp recordings. The responses of a neuron to trains of wide-field blue light pulses at a constant frequency (20 mW at 470 nm, 5 Hz, and 1 ms) were represented.

(F) The amounts of NE release after 15 min illumination with continuous wide-field blue light (26 mW/mm^2 at 488 nm), or no light, were analyzed by using a commercial ELISA kit (*p < 0.05; unpaired Student's t test; and n = 3).

(G and H) Top panels: schematic diagrams for the control of beating rate of NMVM. (G) Increased beating rates were observed upon the photoactivation of hChR2-expressing sympathetic neurons with continuous wide-field blue light (see Experimental Procedures; 26 mW/mm^2 at 488 nm; **p < 0.01; ***p < 0.001; unpaired Student's t test; and n = 5 for *i*, n = 14 for *ii*, n = 14 for *iii*, and n = 13 for *iv*).

(H) Before and after treatment of β-blocker (1 μM propranolol) for 5 min, neuronal-photostimulation-induced beating rate change on NMVM was measured (*p < 0.05; unpaired Student's t test; and n = 3). The orange arrows connect the data, before and after treatment of 1 μM propranolol, obtained from the same NMVM syncytium. The red lines indicate each mean value.

(I) Photoactivation of hChR2-expressing sympathetic neurons co-cultured with NMVM using continuous wide-field blue light or continuous focal blue light. Different from conventional wide-field illumination, the field diaphragm in the epi-illumination pathway of the microscope was fully closed in order to achieve focal illumination (area, 0.08 mm^2). The light intensity was 26 mW/mm^2 at 488 nm. Example images representing focal and wide-field illumination are shown (left). The blue dotted circle indicates an illuminated region with blue light. The white dotted circle indicates a beating region of NMVM. With focal (n = 3) or wide-field (n = 3) illumination, spontaneous beating rates were measured in the order of three sections (~20 s each): (1) "no illumination just before photostimulation", (2) "blue light illumination for photostimulation", and (3) "no illumination just after photostimulation" (right).

All of the error bars represent mean + SEM. The scale bars represent 100 μm. See also Figure S5 and Movie S4.

connections between neurons and NMVM are important to affect the beating rate of NMVM. In addition to the chronotropic effect of nicotine, inotropic effect was also detected on this co-culture system (Figure S4L). Moreover, we found that nicotine treatment in co-culture caused a slight, but significant AP shortening (Figure S4M). In contrast, the propagation of APs and beating synchronization were not altered after neuronal stimulation by nicotine (Movies S2 and S3).

Optogenetic Neural Control of Cardiac Ventricular Myocytes

To test whether their neuronal activity can be controlled by optogenetic stimulations, we transduced PHOX2B::eGFP+ neurons with lentiviral vectors expressing hChR2-eYFP (Figures 5A–5F, S5A, and S5B). hChR2-eYFP expression in TH-positive putative sympathetic neurons were confirmed by immunostaining (Figures 5B–5D). In addition, hChR2-expressing neurons fired

light-induced APs over a broad frequency range from 1 to 10 Hz (Figures 5E and S5B). Spike fidelity was increased with increasing light intensity (Figure S5A). Furthermore, photostimulation in the hChR2-expressing PHOX2B::eGFP+ sympathetic neurons led to NE secretion (Figure 5F). Next, we test whether spontaneous beating rates of co-cultured NMVM with human sympathetic neurons can be controlled optogenetically. The beating rate of NMVM could be optogenetically controlled with hChR2-expressing hESC-derived sympathetic neurons when they were in physical contact with cardiomyocytes (Figure 5G, iii; Movie S4). Following optogenetic activation of neurons, the beating rates of NMVM were quickly dialed up, while immediately down after stimulation (Figure 5I; Movie S4). In contrast, there was no response to light exposure in any of the three control groups: NMVM only (Figure 5G, i), eGFP-expressing neuron with NMVM (Figure 5G, ii), or stimulating non-connected neuron with NMVM (Figure 5G, iv). However, the optogenetic stimulation-induced beating rate increment of NMVM was significantly blocked by the β-blocker, propranolol (Figures 5H and S5C). These data demonstrate that PHOX2B::eGFP+ neurons form physical and functional connections with ventricular myocytes, and these β-adrenergic connections allow pharmacological and optogenetic control of the PHOX2B::eGFP+ neurons to influence cardiac contractile behaviors.

Physical Interaction Leads to Neuronal Maturation Phenotypes

Functional connections between neurons and their target tissues are known to promote neuronal maturation during development (Bharmal et al., 2001; Devay et al., 1999). To test these, we analyzed the ability of the PHOX2B::eGFP+ neurons to release neurotransmitters when co-cultured with or without NMVM. The co-cultured neurons released significantly more NE and expressed significantly higher levels of enzymes crucial for catecholamine synthesis than did neurons cultured without NMVM (Figures 6A, 6B, and S6A). In addition, the expression of nAChRs and sodium and potassium channels were significantly increased in the co-cultured neurons with NMVM compared to those cultured alone (Figures 6C and S6D), which is consistent with the enhanced sensitivity to nicotine (0.1 μM) (Figures 6D–6G; Movie S5). Furthermore, the expression levels of catecholamine-synthesizing enzymes and nAChRs were significantly higher in the co-cultured neurons with NMVM than in control neurons cultured under NMVM-conditioned medium (Figures 6B and 6C). This indicates that the physical contact between the sympathetic neurons and NMVM promotes neuronal maturation. This phenotype was not observed in hPSC-derived sensory neurons co-cultured with NMVM (Figures S6B and S6C). The profiling of mouse sympathetic neurons at different developmental stages showed that expression of these genes is indeed increased during sympathetic maturation in vivo (Figures S6E and S6F). Interestingly, using isolated samples from different regions of microfluidic chambers (Figure S6G), we found that expression levels of these genes were significantly higher in the neurons isolated from the proximal region (closer to NMVM) than the distal region (far from NMVM), implying that the higher probability of direct contact, the higher neuronal maturation occurs (Figures S6H and S6I). On the other hand, the co-cultured NMVM showed significant transcriptional changes of different cardiac marker genes (Fig-

ure S6J), indicating that the co-culturing with sympathetic neurons might affect the cellular phenotype of NMVM. However, the co-culture condition did not change the state of cardiomyocytes itself, including spontaneous beating rates, cell densities, and degrees of cell fusion status (Figures S6K–S6M). Overall, these data suggest that hPSC-derived sympathetic neurons undergo maturation when they are functionally and physically connected with ventricular myocytes.

DISCUSSION

Previous reports demonstrated that hPSCs could be directed into multiple cell types, including neurons (Brennand et al., 2011; Dimos et al., 2008; Li et al., 2005; Maroof et al., 2010) and cardiomyocytes (Laflamme et al., 2007). However, modeling intercellular physiology with hPSCs remains a challenge owing to the absence of a proper model system. In the present study, we demonstrated the sequential development of human sympathetic neurons with four independent genetic reporter hPSC lines engineered by CRISPR/Cas9 technology (Cong et al., 2013; Mali et al., 2013), and the hPSC-derived sympathetic neuron's physical and functional connectivity with cardiac muscle cells (ventricular myocytes). The direct differentiation and prospective isolation of sympathetic neurons from hPSCs described here is to sufficiently model their stepwise development and functional connection on cardiac syncytia. This approach offers unique opportunities for in vitro modeling human sympathetic neurons in the context of mechanistic insight on human neuronal development and interaction with their target tissues under physiological and pathophysiological conditions.

Like migrating sympathoadrenal neural crests in developing animal embryos (Morikawa et al., 2009; Saito et al., 2012; Schneider et al., 1999), activation of SHH and BMP signaling pathways appears crucial for our sympathetic neuronal specification with hPSC-based system (Figures 1G–1J, S1C, and S1D), which allows us to recapitulate human sympathetic neuron specification in vitro. Our characterization of the in vitro molecular profile and functional properties shows that they are similar to those of their in vivo counterparts, including the expression of autonomic/sympathetic marker genes, catecholaminergic enzymes, capacity for NE-release, and electrophysiological profiles, such as phasic/tonic APs and medium AHP (Figures 1L, 2E–2H, 3B–3I, 5E, 5F, S2D, S3A–S3I, and S3L–S3V). Interestingly, small numbers of NMVM showed decreased beating rates after neuronal stimulation with nicotine (Figure 4D, iii), and a subset of PHOX2B::eGFP+ cells co-expressed cholinergic marker genes along with catecholaminergic markers (Figure S4O). Therefore, we speculate that our PHOX2B::eGFP+ cells exhibit functional cholinergic feature, potentially explaining the results of Figure 4D, iii. It will be intriguing to determine how hPSCs can sub-specify into other autonomic neuronal sub-lineages, including parasympathetic neurons and enteric neurons, with additional extrinsic morphogens and signaling cues, or different progenitors, such as peripheral glial cells (Dyachuk et al., 2014; Gershon, 2010).

Modeling diseases of the ANS for personalized medicine has been challenging. Our PHOX2B::eGFP+ neuronal population provides a unique tool with which to dissect the molecular
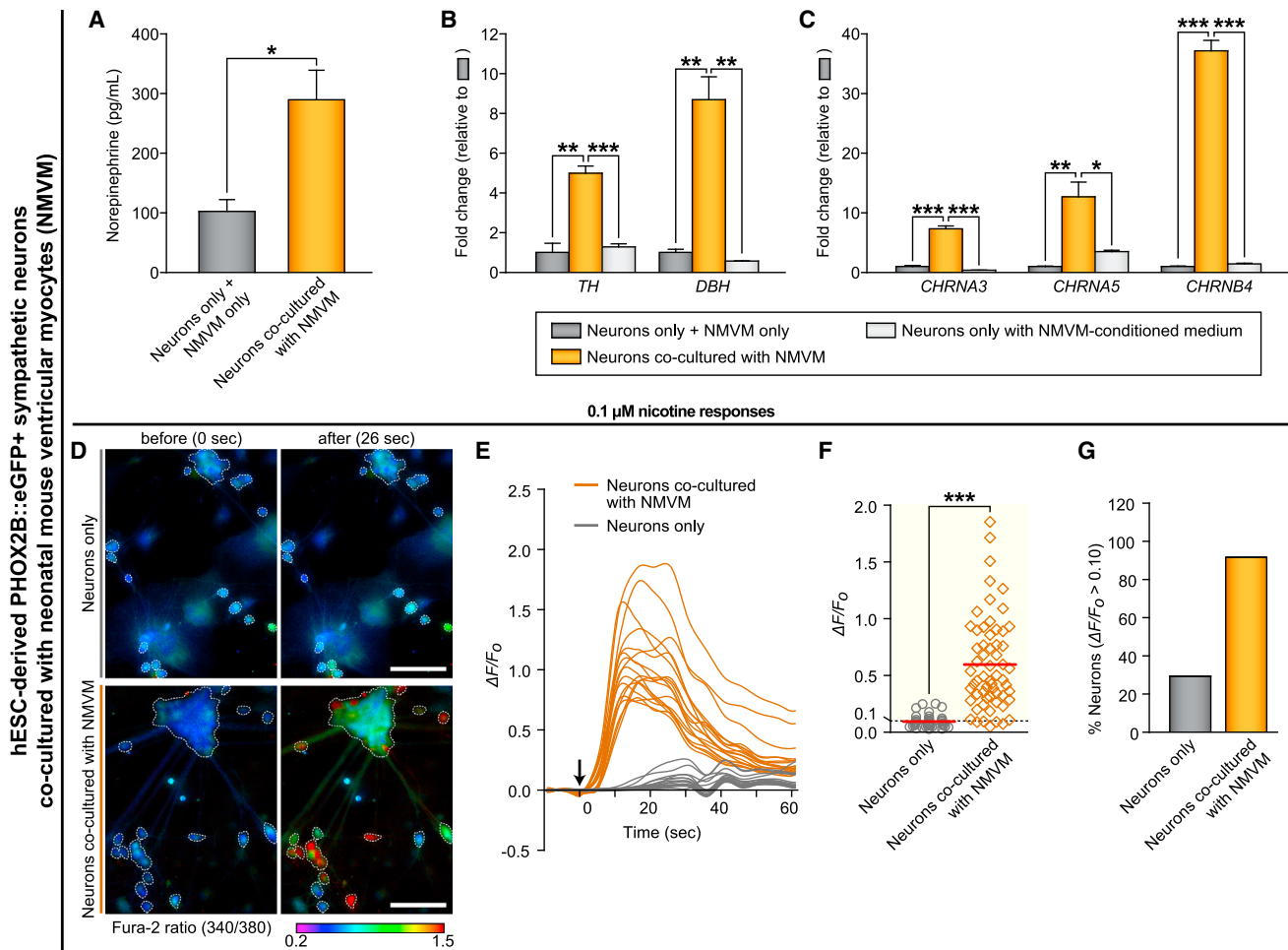
Figure 6. Physical Interaction between hPSC-Derived Sympathetic Neurons and Ventricular Myocytes Leads to Neuronal Maturation Phenotypes

(A) The amounts of NE release after 50 mM KCl administration were analyzed by using a commercial ELISA kit (*$p < 0.05$; unpaired Student's t test; and n = 3) (neurons, hESC-derived PHOX2B::eGFP+ sympathetic neurons, and NMVM).

(B and C) We used the "neurons only with NMVM-conditioned medium" control (1 day conditioned medium of NMVM was collected and fed to neuron only sample daily for 7 days). The RNA from neurons only samples and "NMVM only" samples were mixed together and used as a "neurons only + NMVM only" control. qRT-PCR analyses were performed by using indicated human-specific primers (*$p < 0.05$; **$p < 0.01$; ***$p < 0.001$; unpaired Student's t test; and n = 3).

(D–G) The changes in intracellular calcium concentrations $[Ca^{2+}]_i$ induced by 0.1 μM nicotine were measured by ratiometric Fura-2 imaging. The calcium responses were calculated as the ratio of Fura-2 light emission on excitation at 340 and 380 nm (340/380) or the normalized ratio ($\Delta F/F_0$; $\Delta F = (F - F_0)$, F = the 340/380 at a given time point, F_0 = the mean basal, and unstimulated 340/380 of each cell). The white boundaries in (D) indicate the cell bodies of neurons, which satisfy the criterion for selecting neurons as described in Supplemental Information.

(E) Example traces of $\Delta F/F_0$ intensity from the neurons co-cultured with (dark orange lines) or without (gray lines) NMVM exposed to 0.1 μM nicotine. Each trace is a response from a unique cell (n = 18).

(F) $\Delta F/F_0$ intensity plot showing the response of individual cells to 0.1 μM nicotine (***$p < 0.001$; unpaired Student's t test; neurons only, n = 41; and neurons with cardiomyocytes, n = 60). The red lines indicate each mean value.

(G) The percent of total responder neurons ($\Delta F/F_0$ > threshold) in each sample.

All of the error bars represent mean + SEM. See also Figure S6 and Movie S5.

and cellular aspects of sympathetic specification under physiological conditions, as well as in the presence of congenital autonomic disorders. Our cell specification system can be readily applicable to disease-specific hiPSCs, which will allow us to generate and characterize sympathetic neurons from patients carrying genetic mutations that affect autonomic development and function (Axelrod et al., 2002; Chaudhuri, 2001; Kimura et al., 2012; Mudd and Kass, 2008; Rotthier et al., 2012; Vinik et al., 2003).

The ability of sympathetic neurons to control the behaviors of target tissues also provides an opportunity through which to understand neural modulation. As demonstrated in Figures 4B, 4C, and S4A–S4I, our hPSC-derived PHOX2B::eGFP+ sympathetic neurons can physically associate with cardiac tissues, and ultrastructural analysis shows that putative synaptic vesicles are located in the distal part of the neurons, resembling the early stage of neuromuscular synaptic formation. In addition, pharmacological stimulation (by nicotine treatment) or optogenetic

stimulation (by optical control of channelrhodopsin) of our hPSC-derived PHOX2B::eGFP+ sympathetic neurons increased the beating rate of the connected cardiac syncytia (Figures 4D and 5G). However, hPSC-derived cardiomyocytes co-cultured with human sympathetic neurons did not show a detectable response to neuronal stimulation (with pharmacological stimulation, n = 12, data not shown). Potential explanation for this issue could be because: (1) the co-culture condition may not be sufficient to make functional connections between hPSC-derived cardiomyocytes and human sympathetic neurons, (2) hPSC-derived cardiomyocytes may be still immature to make a functional connection with sympathetic neurons, and (3) hPSC-derived sympathetic neurons may be still immature to make a functional connection with hPSC-derived cardiomyocytes. Further study to determine the suitable co-culture condition and aging/maturation of neurons and cardiomyocytes will be of great interest. Multiple target tissues are controlled by the sympathetic system, and it will be interesting to see whether our PHOX2B::eGFP+ sympathetic neurons, in conjunction with the autonomic circuitry of the CNS, can be connected to, and regulate, the other target organs and tissues, such as blood vessels, bone marrow, and brown adipocytes (Katayama et al., 2006; Perino et al., 2014; Takahashi et al., 2013). Thus it can be used to study the mechanisms of neuronal innervation and to model diseases resulted from pathologic sympathetic activation.

Another interesting finding in the co-culture of PHOX2B::eGFP+ sympathetic neurons and cardiac syncytia was that these functional connections confer maturation phenotypes on the cultured neurons (Figure 6). This observation is in agreement with previous studies in animal models (Onténiente et al., 1992; Sheen et al., 1999), where functional connections of neurons with target organs can lead to neuronal maturation. Likewise, we noticed increased sensitivity to nicotine and elevated levels of both catecholaminergic enzyme expression and NE secretion (Figure 6). These maturation phenotypes elicited by functional connections between human sympathetic neurons and ventricular myocytes can provide insights into maturation of hPSC-derived neurons, which previously has been a challenge, limiting the modeling of neurodegenerative disorders and transplantation with "age-matching" cells (Saha and Jaenisch, 2009). Because hESCs remain at the preimplantation stage, and the reprogramming of somatic cells into hiPSCs resets "biological clocks", the hESC- and hiPSC-derived neurons can be mostly in embryonic and fetal stages. Therefore, functional interaction between the neurons and target tissues could be a "natural" stimulating cue for the neuronal maturation process, as presented in our data (Figure 6). Complementary to the approach using overexpressing progerin, a truncated form of lamin A, which provides a model for understanding the epigenetic and genetic mechanisms underlying neural maturation (Miller et al., 2013), our findings will broaden understanding of human neuronal development as well as the general stem cell field in the context of modeling post-natal, even late onset, neural disorders.

In summary, our study provides a framework for the generation of distinct peripheral sympathetic neurons and an in vitro platform for "sympathetic-cardiac neuromodulation in a dish", to study the neuronal regulation of cardiac behaviors implicated in many cardiac and autonomic diseases.

EXPERIMENTAL PROCEDURES

Isolation of NMVM

NMVM were isolated from 1-day-old C57BL/6 mice ventricles. In brief, the heart was quickly removed from the chest and rinsed one time with 70% EtOH and PBS. After removal of lung tissue, larger vessels, and atria under stereomicroscope, we chopped the ventricles and transferred small pieces of ventricles into a 50 ml conical tube with digestion buffer (for enzymatic digestion, collagenase type II [0.4 mg/ml, Worthington] and pancreatin [0.2 mg/ml, Sigma-Aldrich] were added into the isolation solution [116 mM NaCl, 5.4 mM KCl, 5.5 mM glucose, 0.8 mM $MgSO_4$, 1 mM NaH_2PO_4, and 20 mM HEPES, adjusted to pH 7.4 with NaOH]). Then, put the tube in 37°C water bath for 30 min with shaking. Enzymes were inactivated after NMVM isolation by adding the mouse cardiomyocytes medium, which contains DMEM and Medium 199 in a 4:1 ratio, supplemented with 10% FBS and 1% penicillin/streptomycin.

Pharmacological Control of Spontaneous Beating Rates of NMVM

Measurement of the spontaneous beating rate was performed as described previously (Devic et al., 2001) with slight modifications. In brief, 1–2 × 10^5 isolated NMVM (5 × 10^5 for optical mapping) were added onto hESC-derived sympathetic neurons (4–15 days after PHOX2B::eGFP+ sorting), sensory neurons, or mock with 1:1 mixed medium (mouse cardiomyocytes medium: neuron medium). At 7–9 days after co-culture, the culture plates were placed in a temperature regulation apparatus positioned on the stage of an inverted microscope (Eclipse TE2000-E). Cells were equilibrated at 37°C for 10 min before monitoring the beating rate. A syncytium physically connected with neurites was selected for recording. For calculating beating rates of cells within the syncytium, a video was recorded for 1 min each before and 6 min after the stimulation of hESC-derived sympathetic neurons by 1 μM (-)-nicotine hemisulfate (Sigma-Aldrich). The data were analyzed using Prism.

Optogenetic Control of Spontaneous Beating Rates of NMVM

Optogenetic approaches were performed by using humanized channelrhodopsin-2 (hChR2)-infected hESC-derived sympathetic neurons. After packaging hChR2 lentivirus using pLenti-EF1a-hChR2(H134R)-EYFP-WPRE construct (Addgene plasmid #20942), hESC-derived sympathetic neurons (1–2 days after PHOX2B::eGFP+ sorting) were infected with hChR2 or eGFP lentivirus. The efficiency was checked by YFP or eGFP expression under fluorescence microscope. For eliminating residual virus particles on the well, infected wells were repetitively washed with culture medium and cultured further with changing medium daily for at least 2 days. Then, 1–2 × 10^5 isolated neonatal mouse cardiomyocytes were added onto lentivirus-infected hESC-derived sympathetic neurons (total 4–15 days after PHOX2B::eGFP+ sorting) or mock, with 1:1 mixed medium (mouse cardiomyocytes medium: neuron medium). At 7–8 days after co-culture, the culture plates were placed in a temperature regulation apparatus positioned on the stage of an inverted microscope (Eclipse TE2000-E). Cells were equilibrated at 37°C for 10 min before monitoring the beating rate. For calculating beating rates of cells within the syncytium, a video was repetitively recorded before and after illumination with continuous wide-field blue light (26 mW/mm^2 at 488 nm) for ~20 s. Light intensity was measured on the focal plane with an optical power meter (LaserCheck, Coherent). The data were analyzed using Prism.

ACCESSION NUMBERS

The accession number for the microarray data reported in this paper is GEO: GSE80689.

SUPPLEMENTAL INFORMATION

Supplemental Information includes Supplemental Experimental Procedures, six figures, one table, and five movies and can be found with this article online at http://dx.doi.org/10.1016/j.stem.2016.05.002.

AUTHOR CONTRIBUTIONS

Conceptualization, Y.O., C.K., and G.L.; Methodology, Y.O., G.-S.C., Z.L., I.H., R.Z., M.-J.K., Y.J.K., E.T., L.T., R.H., X.D., C.K., and G.L.; Formal Analysis,

REFERENCES

Anderson, D.J., Groves, A., Lo, L., Ma, Q., Rao, M., Shah, N.M., and Sommer, L. (1997). Cell lineage determination and the control of neuronal identity in the neural crest. Cold Spring Harb. Symp. Quant. Biol. 62, 493–504.

Anderson, R.L., Jobling, P., and Gibbins, I.L. (2001). Development of electrophysiological and morphological diversity in autonomic neurons. J. Neurophysiol. 86, 1237–1251.

Axelrod, F.B., Goldberg, J.D., Ye, X.Y., and Maayan, C. (2002). Survival in familial dysautonomia: Impact of early intervention. J. Pediatr. 141, 518–523.

Bharmal, S., Slonimsky, J.D., Mead, J.N., Sampson, C.P., Tolkovsky, A.M., Yang, B., Bargman, R., and Birren, S.J. (2001). Target cells promote the development and functional maturation of neurons derived from a sympathetic precursor cell line. Dev. Neurosci. 23, 153–164.

Bhatt, S., Diaz, R., and Trainor, P.A. (2013). Signals and switches in mammalian neural crest cell differentiation. Cold Spring Harb. Perspect. Biol. 5, a008326.

Brennand, K.J., Simone, A., Jou, J., Gelboin-Burkhart, C., Tran, N., Sangar, S., Li, Y., Mu, Y., Chen, G., Yu, D., et al. (2011). Modelling schizophrenia using human induced pluripotent stem cells. Nature 473, 221–225.

Chambers, S.M., Fasano, C.A., Papapetrou, E.P., Tomishima, M., Sadelain, M., and Studer, L. (2009). Highly efficient neural conversion of human ES and iPS cells by dual inhibition of SMAD signaling. Nat. Biotechnol. 27, 275–280.

Chambers, S.M., Qi, Y., Mica, Y., Lee, G., Zhang, X.J., Niu, L., Bilsland, J., Cao, L., Stevens, E., Whiting, P., et al. (2012). Combined small-molecule inhibition accelerates developmental timing and converts human pluripotent stem cells into nociceptors. Nat. Biotechnol. 30, 715–720.

Chaudhuri, K.R. (2001). Autonomic dysfunction in movement disorders. Curr. Opin. Neurol. 14, 505–511.

Cong, L., Ran, F.A., Cox, D., Lin, S., Barretto, R., Habib, N., Hsu, P.D., Wu, X., Jiang, W., Marraffini, L.A., and Zhang, F. (2013). Multiplex genome engineering using CRISPR/Cas systems. Science 339, 819–823.

Cunningham, M., Cho, J.H., Leung, A., Savvidis, G., Ahn, S., Moon, M., Lee, P.K., Han, J.J., Azimi, N., Kim, K.S., et al. (2014). hPSC-derived maturing

GABAergic interneurons ameliorate seizures and abnormal behavior in epileptic mice. Cell Stem Cell 15, 559–573.

Devay, P., McGehee, D.S., Yu, C.R., and Role, L.W. (1999). Target-specific control of nicotinic receptor expression at developing interneuronal synapses in chick. Nat. Neurosci. 2, 528–534.

Devic, E., Xiang, Y., Gould, D., and Kobilka, B. (2001). Beta-adrenergic receptor subtype-specific signaling in cardiac myocytes from beta(1) and beta(2) adrenoceptor knockout mice. Mol. Pharmacol. 60, 577–583.

Dimos, J.T., Rodolfa, K.T., Niakan, K.K., Weisenthal, L.M., Mitsumoto, H., Chung, W., Croft, G.F., Saphier, G., Leibel, R., Goland, R., et al. (2008). Induced pluripotent stem cells generated from patients with ALS can be differentiated into motor neurons. Science 321, 1218–1221.

Dyachuk, V., Furlan, A., Shahidi, M.K., Giovenco, M., Kaukua, N., Konstantinidou, C., Pachnis, V., Memic, F., Marklund, U., Müller, T., et al. (2014). Neurodevelopment. Parasympathetic neurons originate from nerve-associated peripheral glial progenitors. Science 345, 82–87.

Gershon, M.D. (2010). Developmental determinants of the independence and complexity of the enteric nervous system. Trends Neurosci. 33, 446–456.

Hirsch, M.R., Tiveron, M.C., Guillemot, F., Brunet, J.F., and Goridis, C. (1998). Control of noradrenergic differentiation and Phox2a expression by MASH1 in the central and peripheral nervous system. Development 125, 599–608.

Huber, K. (2015). Segregation of neuronal and neuroendocrine differentiation in the sympathoadrenal lineage. Cell Tissue Res. 359, 333–341.

Huber, K., Brühl, B., Guillemot, F., Olson, E.N., Ernsberger, U., and Unsicker, K. (2002). Development of chromaffin cells depends on MASH1 function. Development 129, 4729–4738.

Jobling, P., and Gibbins, I.L. (1999). Electrophysiological and morphological diversity of mouse sympathetic neurons. J. Neurophysiol. 82, 2747–2764.

Joseph, N.M., and Morrison, S.J. (2005). Toward an understanding of the physiological function of mammalian stem cells. Dev. Cell 9, 173–183.

Katayama, Y., Battista, M., Kao, W.M., Hidalgo, A., Peired, A.J., Thomas, S.A., and Frenette, P.S. (2006). Signals from the sympathetic nervous system regulate hematopoietic stem cell egress from bone marrow. Cell 124, 407–421.

Kimura, K., Ieda, M., and Fukuda, K. (2012). Development, maturation, and transdifferentiation of cardiac sympathetic nerves. Circ. Res. 110, 325–336.

Laflamme, M.A., Chen, K.Y., Naumova, A.V., Muskheli, V., Fugate, J.A., Dupras, S.K., Reinecke, H., Xu, C., Hassanipour, M., Police, S., et al. (2007). Cardiomyocytes derived from human embryonic stem cells in pro-survival factors enhance function of infarcted rat hearts. Nat. Biotechnol. 25, 1015–1024.

Lee, G., Kim, H., Elkabetz, Y., Al Shamy, G., Panagiotakos, G., Barberi, T., Tabar, V., and Studer, L. (2007). Isolation and directed differentiation of neural crest stem cells derived from human embryonic stem cells. Nat. Biotechnol. 25, 1468–1475.

Li, X.J., Du, Z.W., Zarnowska, E.D., Pankratz, M., Hansen, L.O., Pearce, R.A., and Zhang, S.C. (2005). Specification of motoneurons from human embryonic stem cells. Nat. Biotechnol. 23, 215–221.

Mali, P., Yang, L., Esvelt, K.M., Aach, J., Guell, M., DiCarlo, J.E., Norville, J.E., and Church, G.M. (2013). RNA-guided human genome engineering via Cas9. Science 339, 823–826.

Maroof, A.M., Brown, K., Shi, S.H., Studer, L., and Anderson, S.A. (2010). Prospective isolation of cortical interneuron precursors from mouse embryonic stem cells. J. Neurosci. 30, 4667–4675.

Mica, Y., Lee, G., Chambers, S.M., Tomishima, M.J., and Studer, L. (2013). Modeling neural crest induction, melanocyte specification, and disease-related pigmentation defects in hESCs and patient-specific iPSCs. Cell Rep. 3, 1140–1152.

Miller, J.D., Ganat, Y.M., Kishinevsky, S., Bowman, R.L., Liu, B., Tu, E.Y., Mandal, P.K., Vera, E., Shim, J.W., Kriks, S., et al. (2013). Human iPSC-based modeling of late-onset disease via progerin-induced aging. Cell Stem Cell 13, 691–705.

Morikawa, Y., Maska, E., Brody, H., and Cserjesi, P. (2009). Sonic hedgehog signaling is required for sympathetic nervous system development. Neuroreport 20, 684–688.

Mudd, J.O., and Kass, D.A. (2008). Tackling heart failure in the twenty-first century. Nature *451*, 919–928.

Onténiente, B., Nothias, F., Geffard, M., and Peschanski, M. (1992). Maturation and fine structure of thalamic reticular neurons transplanted into the adult rat CNS. Dev. Neurosci. *14*, 130–143.

Pattyn, A., Goridis, C., and Brunet, J.F. (2000). Specification of the central noradrenergic phenotype by the homeobox gene Phox2b. Mol. Cell. Neurosci. *15*, 235–243.

Perino, A., Beretta, M., Kilić, A., Ghigo, A., Carnevale, D., Repetto, I.E., Braccini, L., Longo, D., Liebig-Gonglach, M., Zaglia, T., et al. (2014). Combined inhibition of PI3Kβ and PI3Kγ reduces fat mass by enhancing α-MSH-dependent sympathetic drive. Sci. Signal. *7*, ra110.

Perrier, A.L., Tabar, V., Barberi, T., Rubio, M.E., Bruses, J., Topf, N., Harrison, N.L., and Studer, L. (2004). Derivation of midbrain dopamine neurons from human embryonic stem cells. Proc. Natl. Acad. Sci. USA *101*, 12543–12548.

Rotthier, A., Baets, J., Timmerman, V., and Janssens, K. (2012). Mechanisms of disease in hereditary sensory and autonomic neuropathies. Nat. Rev. Neurol. *8*, 73–85.

Saha, K., and Jaenisch, R. (2009). Technical challenges in using human induced pluripotent stem cells to model disease. Cell Stem Cell *5*, 584–595.

Saito, D., Takase, Y., Murai, H., and Takahashi, Y. (2012). The dorsal aorta initiates a molecular cascade that instructs sympatho-adrenal specification. Science *336*, 1578–1581.

Schneider, C., Wicht, H., Enderich, J., Wegner, M., and Rohrer, H. (1999). Bone morphogenetic proteins are required in vivo for the generation of sympathetic neurons. Neuron *24*, 861–870.

Schrenk-Siemens, K., Wende, H., Prato, V., Song, K., Rostock, C., Loewer, A., Utikal, J., Lewin, G.R., Lechner, S.G., and Siemens, J. (2015). PIEZO2 is required for mechanotransduction in human stem cell-derived touch receptors. Nat. Neurosci. *18*, 10–16.

Sheen, V.L., Arnold, M.W., Wang, Y., and Macklis, J.D. (1999). Neural precursor differentiation following transplantation into neocortex is dependent on intrinsic developmental state and receptor competence. Exp. Neurol. *158*, 47–62.

Steinbeck, J.A., Jaiswal, M.K., Calder, E.L., Kishinevsky, S., Weishaupt, A., Toyka, K.V., Goldstein, P.A., and Studer, L. (2016). Functional connectivity under optogenetic control allows modeling of human neuromuscular disease. Cell Stem Cell *18*, 134–143.

Takahashi, Y., Sipp, D., and Enomoto, H. (2013). Tissue interactions in neural crest cell development and disease. Science *341*, 860–863.

Vinik, A.I., Maser, R.E., Mitchell, B.D., and Freeman, R. (2003). Diabetic autonomic neuropathy. Diabetes Care *26*, 1553–1579.